Arctic Science

OPEN ACCESS | Article

Slow change since the Little Ice Age at a far northern glacier with the potential for system reorganization: Thores Glacier, northern Ellesmere Island, Canada

Will Kochtitzky[a], **Luke Copland**[a], **Trudy Wohlleben**[b], **Pilipoosie Iqaluk**[c], **Catherine Girard**[d], **Warwick F. Vincent**[e], **and Alexander I. Culley**[f]

[a]Department of Geography, Environment and Geomatics, University of Ottawa, Ottawa, ON K1N 6N5, Canada; [b]Ottawa, ON, Canada; [c]Qausuittuq (Resolute Bay), NU, Canada; [d]Département des sciences fondamentales, Centre d'études nordiques (CEN), Université du Québec à Chicoutimi, Chicoutimi, QC G7H 2B1, Canada; [e]Centre d'études nordiques (CEN), Takuvik International Laboratory, Département de biologie, and Institut de Biologie Intégrative et des Systèmes (IBIS), Université Laval, Quebec City, QC G1V 0A6, Canada; [f]Centre d'études nordiques (CEN), Takuvik International Laboratory, Département de biochimie, microbiologie et bio-informatique, and Institut de Biologie Intégrative et des Systèmes (IBIS), Université Laval, Quebec City, QC G1V 0A6, Canada

Corresponding author: **Will Kochtitzky** (email: wkoch063@uottawa.ca)

Abstract

Relatively little is known about the glaciers of northern Ellesmere Island, Canada. Here we describe the first field and remote sensing observations of Thores Glacier, located 50 km inland from the Arctic Ocean. The glacier is slow-moving, with maximum velocities of 26 m a^{-1} and a maximum observed thickness of 360 ± 4.3 m. There has been little change in terminus position since at least 1959, with a maximum advance of 170 m at the northwest terminus ending on land and retreat up to 130 m at the southeast terminus ending in Thores Lake. There is little evidence for change since the Little Ice Age as bedrock weathering patterns suggest retreat of no more than 20–30 m around most of the glacier margin. The supraglacial drainage network is generally poorly developed, without moulins and with few crevasses, and therefore no evidence of water reaching the glacier bed. This is supported by one-dimensional modelling, which suggests current basal temperatures of −7.0 °C to −12.0 °C along the centerline. Thores Glacier currently dams Thores Lake, which causes drainage to flow to the southeast. However, if the glacier thins or retreats sufficiently, regional drainage will reverse and flow to the north, and Thores Lake would no longer exist.

Key words: Arctic, climate change, glaciers, proglacial lake, Little Ice Age, Last ice area

Introduction

The Queen Elizabeth Islands of the northern Canadian Arctic contain the largest area of glacier ice in the world outside Greenland and Antarctica, with a total of ~105 000 km^2 (RGI Consortium 2017). Atmospheric temperatures in this region have rapidly increased recently, with in situ surface mass balance records indicating that annual glacier mass loss rates were approximately five times greater between 2005 and 2009 than 1963 and 2004 (Sharp et al. 2011). Geodetic mass balance measurements also indicate widespread glacier losses across the Queen Elizabeth Islands, with differencing of digital elevation models (DEMs) produced from stereo satellite imagery by Hugonnet et al. (2021) indicating mean thinning of 0.34 ± 0.03 m a^{-1} (mass loss of 30.6 ± 4.8 Gt a^{-1}) across the region over the period 2000–2019. Similarly, Tepes et al. (2021) reported mean mass losses of 32.3 ± 1.6 Gt a^{-1} for this region over the period 2010–2017, based on swath processing of CryoSat-2 satellite altimetry data. Results from satellite gravimetry observations by Ciracì et al. (2020) of glacier mass loss are higher at 41.2 ± 7 Gt a^{-1} for the Queen Elizabeth Islands from 2002 to 2019.

Despite the widespread regional losses in glacier mass, there have been few in situ measurements of land-terminating glaciers and their changes across northernmost Ellesmere Island, particularly in the 21st century. The most detailed studies have focused on locations such as White Glacier, Axel Heiberg Island (e.g., Iken 1974; Blatter 1987; Thomson et al. 2017), and John Evans Glacier, Ellesmere Island (e.g., Copland and Sharp 2001; Bingham et al. 2005), both 300–400 km south of the northern coast of Ellesmere Island. Evans (1989) describes glacial geological observations from land-terminating glaciers in Philips Inlet, NW Ellesmere Island, but made no direct glaciological observations. Braun et al. (2004*a*) and Serreze et al. (2017) have reported on mass losses from ice caps on the Hazen Plateau, to the south of the Northern Ellesmere Icefield, while White and Copland (2018) provided the first measurements of change for the entire Northern Ellesmere Icefield and adjacent ice shelves,

Fig. 1. Thores Glacier system overview. Thores Glacier (73.828°W, 82.677°N) is located ~50 km inland from the Arctic Ocean. Most of the glacier is currently located in the Thores Lake watershed (Fig. 2), which flows southeast towards Disraeli Glacier. If the glacier retreats sufficiently, regional drainage will reverse from the current outflow through Thores River, and instead flow to the north. Image from Landsat 8 on 17 July 2016. Outline of Ellesmere Island from Natural Earth.

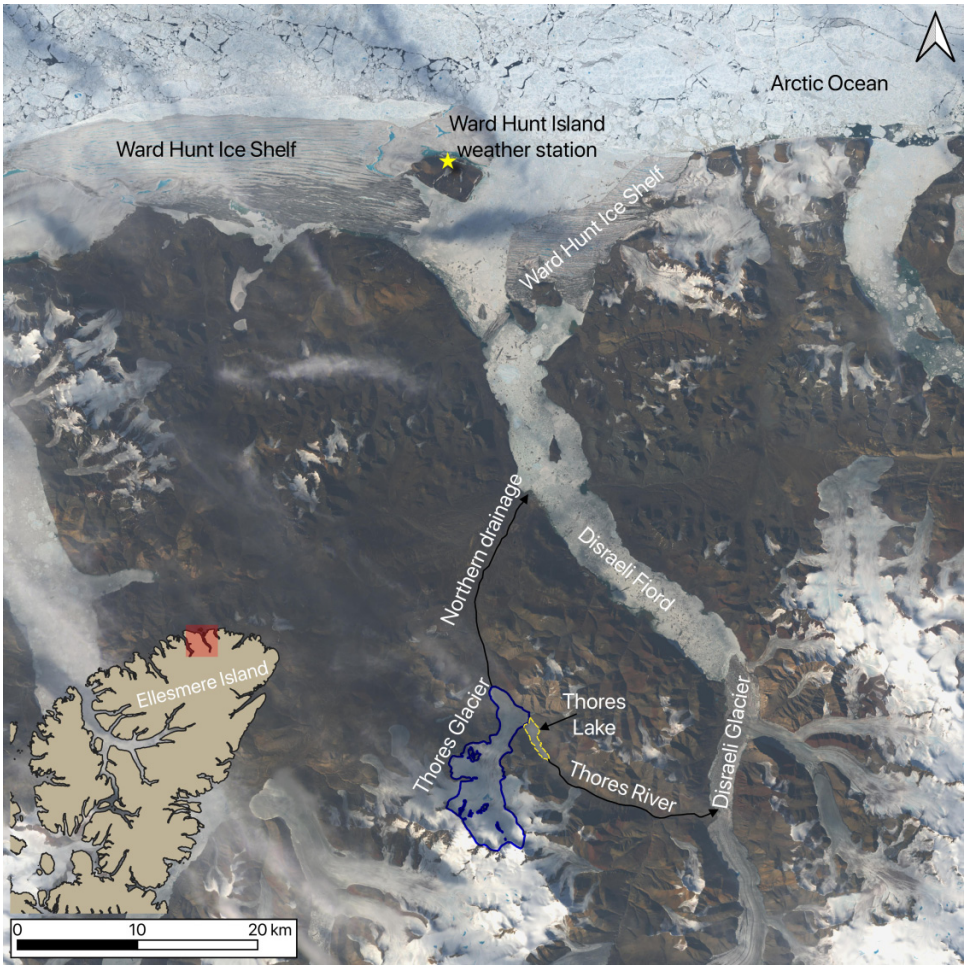

with total area losses of 1705 km^2 (5.9%) over the period 1999–2015.

In this study, we used air photographs, satellite imagery, DEMs, temperature modelling, and field observations including ground penetrating radar (GPR), to provide the first detailed description of the physical properties and recent changes of a land-terminating glacier on far northern Ellesmere Island (Thores Glacier), and to assess its influence on regional hydrology and how this may change in the future (Fig. 1). Thores Glacier lies within the terrestrial margin of the Last Ice Area, so named because it contains the oldest, thickest sea ice in the Arctic and is considered the ultimate refuge for ice-dependent marine species in the warming North (Vincent and Mueller 2020). Large ongoing changes are taking place in the coastal sea ice, ice shelves, and climate of this area (Copland and Mueller 2017; Vincent and Mueller 2020; Newton et al. 2021) that may influence inland temperatures, precipitation, biology, and ice dynamics. Our observations of Thores Glacier, which lies 50 km inland from the Arctic Ocean, therefore provide an assessment of its current status in the face of these regional climate and sea ice changes, and its vulnerability to future change. The glacier is locally significant in that it dams proglacial Thores Lake, which may be one of the few remaining Arctic lakes with multiyear lake ice coverage (Culley et al. 2022). We undertook a suite of field and remote sensing observations on Thores Glacier as part of a broader project to describe the Thores Lake ecosystem and its associated ice environments, and to examine their potential responses to ongoing climate warming. This research is a contribution to the connectivity theme of "Terrestrial Multidisciplinary distributed Observatories for the Study of Arctic Connections" (T-MOSAiC), a project under the auspices of the International Arctic Science Committee that is focused on ocean–land interactions, and system-level responses of terrestrial environments to Arctic climate change (Vincent et al. 2019).

Study area

Thores Glacier (73.828°W, 82.677°N) is located on northern Ellesmere Island (Figs. 1 and 2), 60 km southwest of the northernmost point in Canada, Cape Columbia, and at the

Fig. 2. Thores Glacier characteristics: (A) Thores Glacier with largest supraglacial streams outlined from 1959 air photo and 2019 photo survey. (B) Full extent of the watershed for Thores Lake and the basin for Thores Glacier with the white box displaying the extent of (A). (C) Location of Thores Glacier and Thores Lake in the Arctic (red dot). Base image in (A, B) is from Sentinel-2, 27 July 2021.

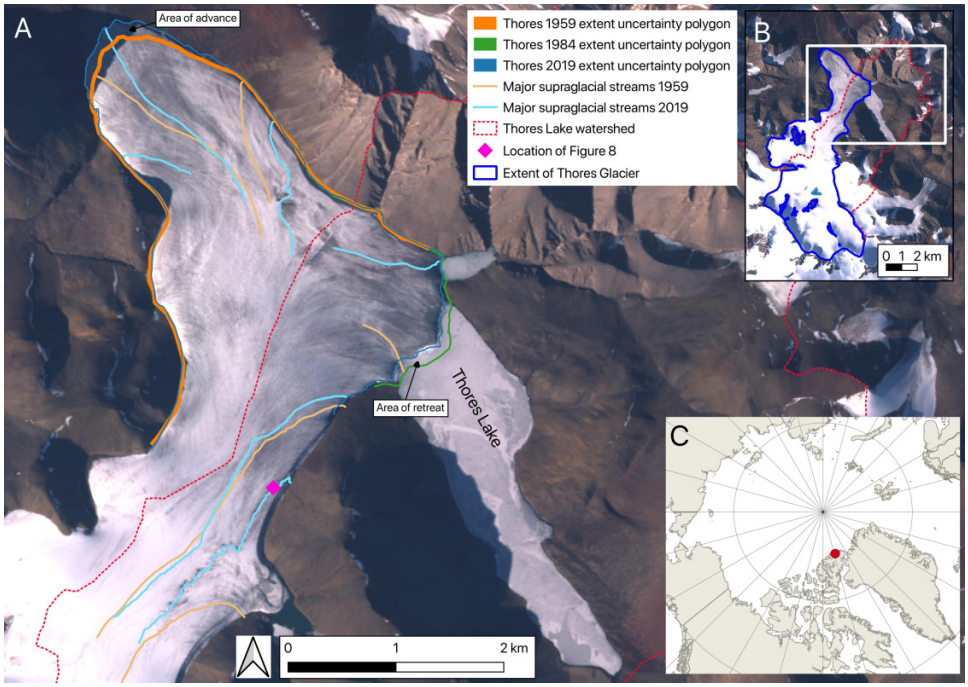

southern end of the Marvin Peninsula (Lemmen 1989). The surrounding polar desert environment is characterized by low annual temperatures and precipitation, and sparsely vegetated catchments dominated by bare rock and glacial deposits (further details in Vincent et al. 2011). The nearest weather station is located on Ward Hunt Island, 44 km to the north of the terminus of Thores Glacier, where air temperatures reach a monthly average maximum of several degrees above freezing in July (CEN 2020; Fig. 3). This weather station has recorded annual temperatures since 2006 (with incomplete data in 2011, 2012, 2015, and 2019 to present). In the available record, the annual average air temperature ranged from −18.0 °C (2013) to −15.4 °C (2017). Snowpack at the Ward Hunt Island site accumulates over fall and winter to a maximum depth of 120–190 cm in May, decreasing to snow-free conditions by July each year with some patches of permanent snow (CEN 2020; Fig. 3). Automated camera observations at Ward Hunt Island show that snowfall occurs intermittently during summer, and snow covers the landscape from September to July (NEIGE 2020).

Thores Glacier has a centerline length of 15 km, with elevations ranging from the terminus at ~300 m above sea level (a.s.l.) to the top of the main accumulation area at ~1200–1300 m a.s.l., although some peaks that define the glacier basin rise to ~1600 m a.s.l. (Fig. 4). The glacier flows generally northwards, and it has a split terminus with one margin that ends in Thores Lake to the southeast, and a second margin that is land-terminating to the northwest (Fig. 2). At present, meltwater coming off Thores Glacier either goes north to the land-terminating margin and towards the north end of Disraeli Fiord, or southeast into Thores Lake.

The Thores Lake outflow currently flows for 30 km, down Thores River, past an unnamed glacier and on to Disraeli Glacier before entering southern Disraeli Fiord that connects to the Arctic Ocean (Fig. 1). Up until 2003, Disraeli Fiord was covered by freshwater ice over an epishelf lake that extended from Disraeli Glacier to the inner edge of the Ward Hunt Shelf, covering about 70 km (Mueller et al. 2003). Over the last two decades, the ice shelf has fractured and collapsed, and the fiord is now covered in sea ice most of the year. Since 2012, there have been occasional late-summer periods of completely open water from Disraeli Glacier to the Arctic Ocean (Copland and Mueller 2017; Vincent and Mueller 2020).

Materials and methods

General glacier characteristics

To understand the general characteristics of Thores Glacier, we used two satellite-derived data sets which cover the glacier and surrounding hydrological basin. To map the glacier area, length, and accumulation area ratio we used a cloud-free, minimal snow Sentinel-2 image of Thores Glacier at 10 m resolution from 27 July 2021. Few earlier satellite images of the glacier are available due to its high latitude, particularly prior to 2015, which puts it beyond the typical coverage of most sensors such as Landsat. To map the hypsometry of the glacier basin, and to help in defining the basin limits, we used tiles 34_37 and 33_37 of the 10 m DEM of the ArcticDEM from

Fig. 3. Ward Hunt weather observations. (Upper) Air temperature observations and (lower) snow depth. Weather station location shown in Fig. 1.

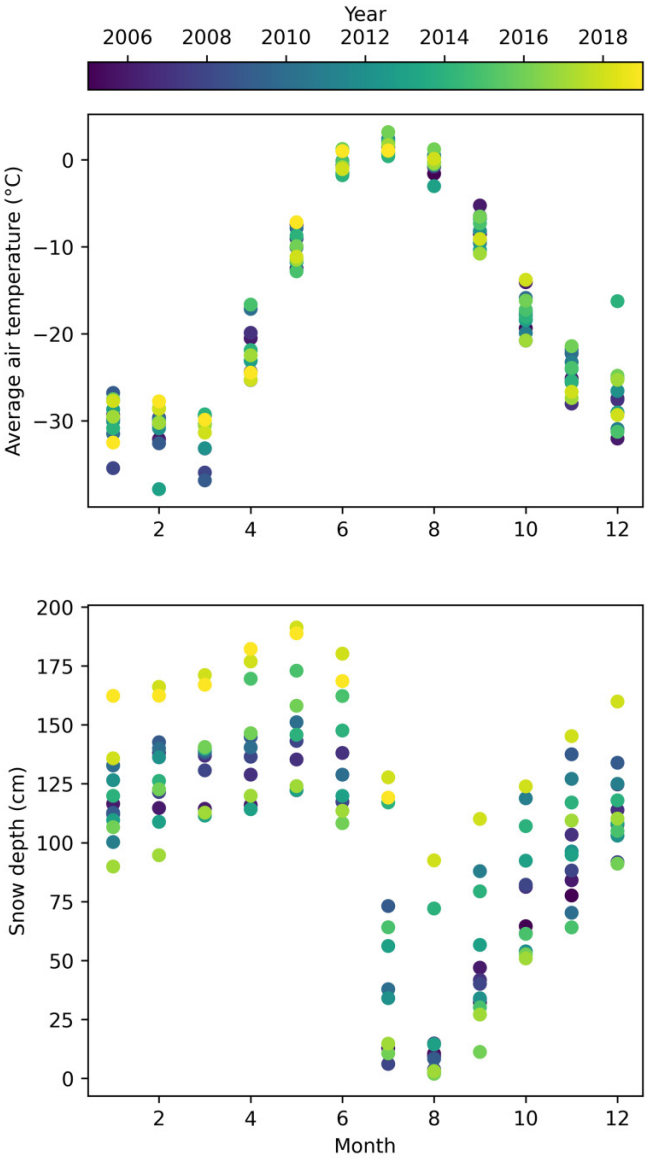

Fig. 4. Elevation of Thores Glaciers. (A) Hypsometry (elevation distribution) of Thores Glacier, in m a.s.l., from the ArcticDEM. The modern equilibrium line altitude is at ~800 m a.s.l., and is marked with a black dotted line. (B) Elevation of Thores Glacier with 100 m contours. White areas are Nunataks within Thores Glacier or not part of the glacier.

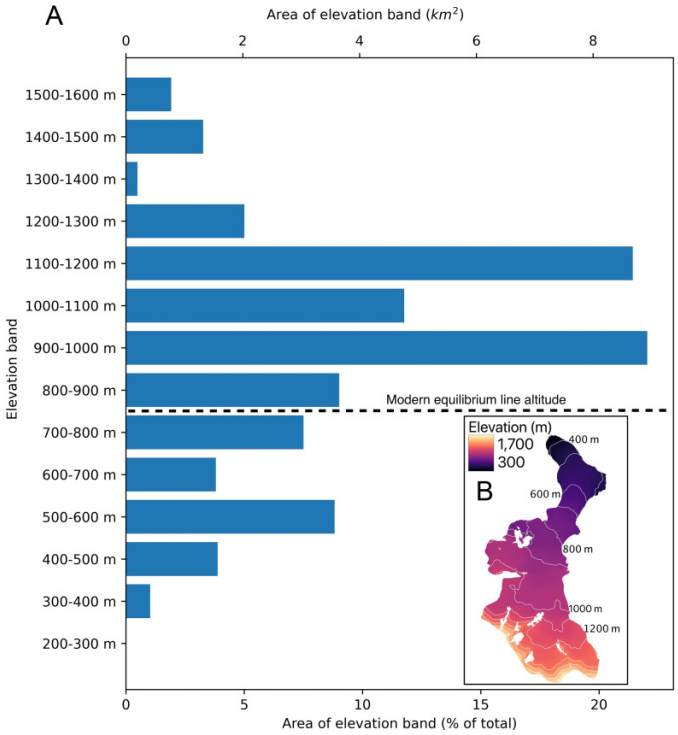

the Polar Geospatial Center (https://www.pgc.umn.edu/data/arcticdem/; Porter et al. 2018). They assembled these tiles from automated stereo matching of WorldView images from 2011 to 2017.

The present-day snowline was determined from the average elevation of the boundary between the snow-covered and snow-free glacier surface in cloud-free, late summer (July to August) satellite imagery from 2016 to 2021. We surmised that this snowline would provide an approximate estimate of the equilibrium line altitude (ELA), while acknowledging that this does not consider the common formation of superimposed ice on the surface of Arctic glaciers below the snowline which can add mass to the glacier. In a study on Devon Ice Cap in the southern Queen Elizabeth Islands, Casey and Kelly (2010) assessed this issue in detail and concluded that the late summer snowline provides the best estimate of the ELA, with a good match between remote sensing-derived and in situ measurements, despite large variations in extent of the superimposed ice zone between years.

Detailed mapping from photogrammetry

To quantify the detailed physical characteristics of Thores Glacier and its interaction with adjacent Thores Lake, we mapped its extent, surface features, surface elevation, and thickness during a July 2019 field campaign. These measurements were limited to the lower part of the glacier (mainly ablation area) due to safety and access limitations. On 28 July 2019, we conducted an air photo survey from a helicopter flying at an altitude of 500–800 m above the glacier (~1100–1200 m a.s.l.) to create an orthomosaic and DEM of the glacier surface using the Structure from Motion technique, following the methodology of Thomson and Copland (2016). We flew the helicopter in sets of parallel lines spaced ~250 m apart across two different sections of the glacier: eight lines were SW–NE trending, parallel to the main trunk of the glacier. Another nine lines were SE–NW trending, approximately perpendicular to the previous flight path and extending from the southern end of Thores Lake to the northwest edge of the glacier terminus.

For the air photo survey a Nikon D850 digital single lens reflex camera with a 24 mm lens was used to capture nadir

photographs every 3 s with an intervalometer, with approximately 60% horizontal overlap between adjacent images. We determined the location of each photograph using a Trimble R7 dual-frequency global positioning system (GPS) which recorded 10 positions per second, with data post-processed using the Natural Resources Canada Precise Point Positioning tool (webapp.geod.nrcan.gc.ca/geod/tools-outils/ppp.php). The camera placed an event marker in the GPS record each time a photograph was taken, and we wrote a custom Python script (available from https://github.com/willkochtitzky/photostodem) to calculate the position of each photograph based on linear interpolation between GPS positions. The processing technique assumes that the path of the aircraft is linear on a 0.1 s timescale. The photographs, with spatial coordinates, were then ingested into Agisoft Metashape Pro version 1.6.3 and processed to create a 0.5 m resolution orthomosaic and a 1 m resolution DEM of the surveyed area. Based on the output report from the Metashape processing, we estimate the positional uncertainty of the DEM and orthomosaic to be 1.7 m along the *x* direction, 1.9 m along the *y* direction, and 4.9 m in the *z* direction for a total uncertainty of 5.5 m.

Changes from 1950s to present day

To quantify long-term changes at Thores Glacier, we mapped distinctive supraglacial streams and the perimeter of the glacier below the snowline in air photographs from 1959 and 1984, and in our 2019 orthomosaic. All digitization was undertaken manually in QGIS 3.10 in the WGS84 UTM 18 N projection (EPSG 32618).

The 26 July 1959, nadir air photo (number A16694-112) was taken by the Royal Canadian Air Force and accessed through the National Air Photo Library, Ottawa, Canada. We georeferenced the photograph to our 2019 orthomosaic with 11 well-distributed tie points on stable features such as distinctive river valleys, boulders, and mountain tops. We applied a second-order polynomial fit between the manually selected coordinates and the ground truth points to warp the image for georectification. The final georeferenced 1959 air photograph had a spatial resolution of 4.6 m and positional uncertainty of 3.05 pixels, or 14.1 m. This georectification only applies to the glacier area and surrounding bedrock below ~700 m a.s.l. as the georectification is more uncertain at higher elevations due to fewer available features to use as control points.

We obtained another air photograph from 29 July 1984, from the National Air Photo Library in Ottawa (number A26575-007). This photograph covers almost the entire glacier, with the exception of the outer part of the northwest terminus, and was georectified against our 2019 orthomosaic using the same methodology as the 1959 photo. The final georeferenced 1984 air photo had a spatial resolution of 1.4 m and positional uncertainty of 8.7 m.

The error in the digitization process for glacier area is estimated to be ±1 pixel (Krumwiede et al. 2014), which is 0.0009 km^2 for a 30 m pixel. When added to the georectification error, the uncertainty calculated as root sum squared errors of our manual digitization of the outline of Thores Glacier is 18.8, 8.8, and 6.0 m for the 1959, 1984, and 2019 images, respectively.

Fig. 5. Thores Glacier median surface velocity from 2016 to 2021, overlain on a hillshade using the ArcticDEM for the lower portion of the glacier. Labelled regions indicate locations referred to in the text. Arrows show the relative magnitude and direction of ice motion.

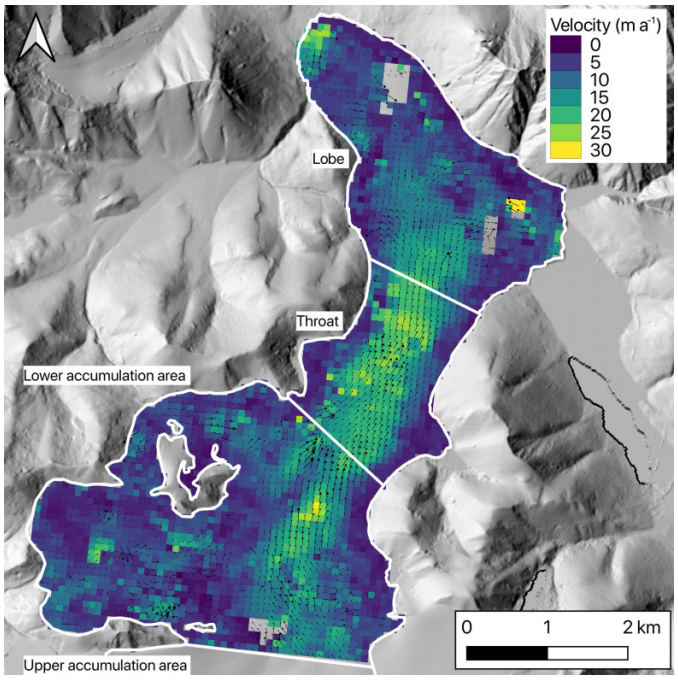

Glacier velocity

To map glacier surface velocity we first downloaded Sentinel-2 cloud-free imagery with minimal snow cover in the ablation area, from July every year between 2016 and 2021 from Earth Explorer (https://earthexplorer.usgs.gov). We used the autonomous repeat image feature tracking (autoRIFT) software (Lei et al. 2021), with default settings of a chip size between 16 and 32 pixels (160–320 m based on the 10 m resolution of Sentinel-2), to derive velocities between images approximately 1 and 2 years apart. For example, we performed the correlation between 2016 and 2017 images, as well as 2016 and 2018. Velocity maps from single image pairs were typically quite noisy due to the generally low ice motion over the study area, so for the final map we took the median of all velocity maps from 2016 to 2021 to create one composite map. The median was used as it is less sensitive to the value of erroneous outliers than the mean (Dehecq et al. 2015). Because this composite still contained noise, we assessed the median velocity in four different areas of Thores Glacier: the lobe (below 630 m a.s.l.), the throat (630–800 m a.s.l.), the lower accumulation area (800–950 m a.s.l.), and the upper accumulation area (above 950 m a.s.l.; Fig. 5).

The uncertainty in the velocity mapping was determined from the median velocity of nearby stable bedrock areas, which do not have seasonal snow, ice, or lake cover. The

median value of apparent motion over these areas was 1.8 m a^{-1}.

Glacier thickness

To map the thickness of Thores Glacier, we used a 25 MHz GPR system from Blue System Integration Ltd., with the transmitter and receiver spaced 9 m apart. We carried out the mapping on 15 July 2019, by walking and towing the GPR system across the ice surface in a sled with leading and trailing antennae. We used a single-frequency GPS receiver to capture the horizontal position of each GPR measurement, and the DEM produced from our photogrammetry survey on 28 July 2019, to determine the surface elevation of each point. We estimate the horizontal accuracy of the GPS position measurements to be 5 m. We processed the data using IceRadarAnalyzer software assuming a radar wave velocity through ice of 0.170 m ns^{-1}, based on previous common midpoint surveys on other ice masses on Ellesmere Island: John Evans Glacier (Copland and Sharp 2001) and the Milne Ice Shelf (Mortimer et al. 2012).

Uncertainty in ice thickness occurs due to variability in travel speed of the radar wave through ice (which we estimate to be ±0.002 m ns^{-1}; Bogorodsky et al. 1985) and the wavelength of the radar system (25 MHz). The variability in radar wave velocity amounts to a maximum ice thickness uncertainty of 4.2 m for the deepest ice measured at Thores Glacier, and 0.68 m for the wavelength uncertainty (10% of the wavelength distance; Bogorodsky et al. 1985). Together, these produce a maximum total uncertainty of 4.3 m assuming that the two sources are uncorrelated, although thinner ice will have less uncertainty.

Basal ice temperatures

We used a one-dimensional (1-D) equilibrium version of an ice temperature model originally developed by Hutter (1993) for predominantly cold glaciers to determine basal temperatures along the centerline of Thores Glacier. Our version of the model has a 20 m vertical resolution and is based on the implementation developed for John Evans Glacier by Wohlleben et al. (2009), where the model is fully described. Ice temperatures, T, neglecting horizontal frictional heating terms related to ice deformation, basal sliding, and subglacial water drainage (justified here by the slow surface velocities, indicative of cold internal temperatures), were calculated using the following equation.

$$\frac{\partial T}{\partial t} = -w\frac{\partial T}{\partial z} + k\frac{\partial^2 T}{\partial z^2}$$

where t is time, k is the thermal diffusion coefficient for ice (assumed to be constant), z is the vertical coordinate, and w is the vertical velocity. The model neglects horizontal thermal diffusion and horizontal advection.

To derive the equilibrium solution, we assumed that $\partial T/\partial t = 0$. Temperatures were modelled for 1-D points using the ice thickness measured with the GPR in 2019. A range of plausible vertical velocities were computed from the surface mass balance results of Noël (2017) and divergence of the horizontal velocity, assuming that vertical motion was negative (i.e., downwards) in the accumulation area and positive (i.e., upwards) in the ablation area. The surface temperature boundary condition was defined using a range of mean annual surface air temperatures of between −16.7 °C (recorded at Ward Hunt Island, 45 km north of Thores Glacier from 2006 to 2018; CEN 2020) and −18.5 °C (recorded at Purple Valley, 100 km west of Thores Glacier, from 2010 to 2018; Copland and Mueller 2021).

As in Hutter (1993), the equilibrium basal boundary condition was taken as $\partial T/\partial z = -G/K$ where the ice-bed interface is below freezing, G is the basal geothermal heat flux of 0.06 W m^{-2} (based on values measured for northern Ellesmere Island; Beltrami and Taylor 1995), and K is the thermal conductivity of the ice of 2.16 W m^{-1} °C^{-1}. In the model the basal boundary condition was constrained to T equal or less than 0 °C if and where it reached the pressure melting point, by assuming that there was little depression in basal melting temperature for the ice depths at Thores Glacier.

Results

Glacier characteristics

Thores Glacier covered an area of 42.7 ± 0.65 km^2 in 2019, with the lowest part of the terminus at 280 m a.s.l. and the top of the accumulation area reaching to ~1200 m a.s.l. If we assume that the end-of-summer snowline was representative of the equilibrium line, then in the 27 July 2021 Sentinel-2 image the accumulation area ratio was 0.77, with the snowline at ~800 m a.s.l. (Figs. 2B and 4). This date is near the end of the typical ablation season of Thores Glacier, and the snowline was at a similar elevation during our late-July 2019 fieldwork, as well as in late-July 2016 and 2020 Sentinel-2 imagery. In the only other years when cloud-free imagery was available, 2017 and 2018, Sentinel-2 showed an even lower snowline. Supraglacial streams incised into the ice were only present below this elevation in all imagery, which supports 800 m a.s.l. as a reasonable measure of the recent ELA.

Our GPR measurements revealed a maximum observed ice thickness of 360 ± 4.3 m at a surface elevation of 800 m a.s.l, near the present-day snowline (Fig. 6). All radargrams showed a clear bed reflection, with little to no internal returns (Fig. 7). The glacier was thinner towards the terminus where it ended in ice cliffs to the northwest (Fig. 8), but more gently sloped into Thores Lake to the southeast without a calving face. While we were unable to directly measure the cliff heights due to safety concerns, ice thicknesses within 300 m of the glacier margin were 90–100 m near the northwest terminus, 40–50 m on the valley wall to the northeast, and 110–120 m near Thores Lake.

Thores Glacier at the time of observation had very few crevasses. Some small crevasses, less than ~1 m wide and ~2 m deep, existed near the Thores Lake margin and one in the middle of the terminal lobe running southwest–northeast. We did not observe crevasses anywhere else on the glacier.

Most streams remained on the glacier surface, although in 2019 we observed a ~50 m stretch of an incised supraglacial stream that went under a snow bridge before re-emerging

Fig. 6. Thores Glacier ice thickness: (A) Thickness profile at approximately the snowline. (B) Thickness profile down the centerline of the glacier. (C) Thickness transects across the terminal lobe. (D) Overview of all thickness observations from Thores Glacier collected on 15 July 2019, with 20 m surface elevation contours. (E) Overview of (A–C) transect locations. Base images in (D, E) is from Sentinel-2 on 27 July 2021. The vertical uncertainty of the GPR thickness measurements is <4.3 m and the horizonal uncertainty is less than the size of the dots (~5 m).

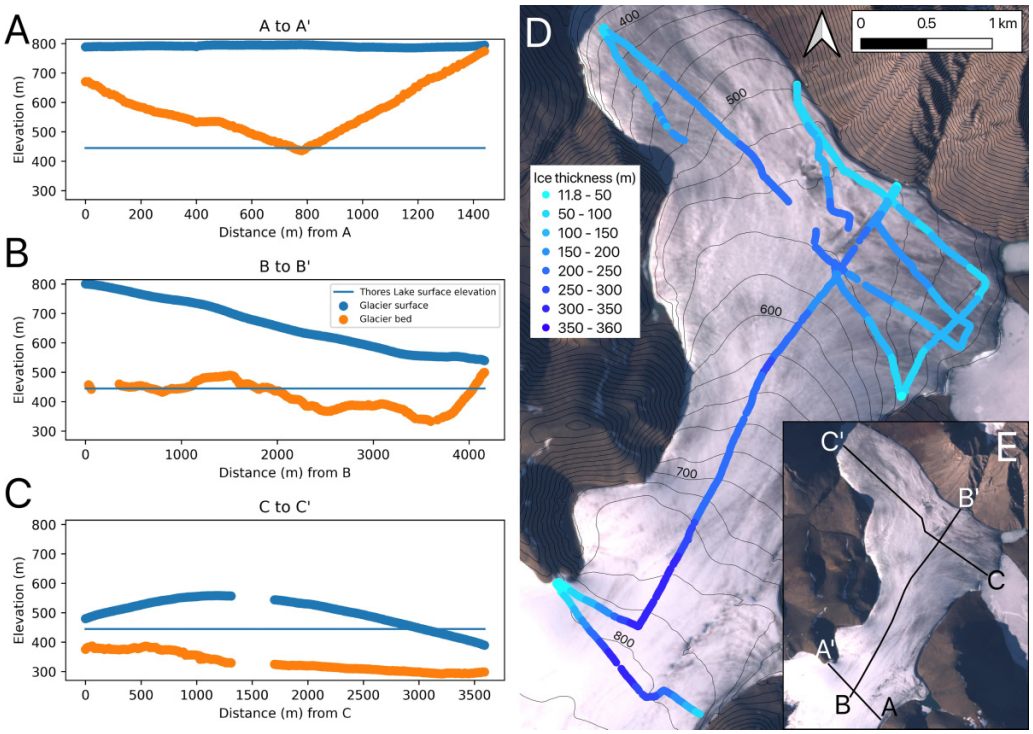

Fig. 7. GPR observations along the centerline of Thores Glacier collected on 15 July 2019, with the bed reflection denoted by a change in colour from grey to yellow. Distance along profile is from point B in Fig. 6E, with Fig. 6B showing the processed data for this transect (with the exception of the final 700 m, which was collected on a different line).

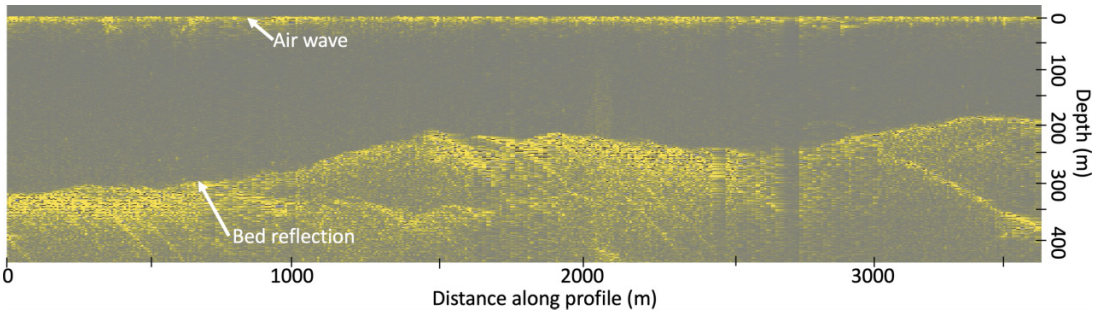

(Fig. 9). Field observations indicate that the supraglacial stream channels were generally narrow (maximum width of ~2 m) and little incised (maximum depth of ~8 m; Fig. 9). The glacier did not have any moulins: we found no evidence of them in the 1959 or 1984 air photographs, in our 2019 photogrammetry survey, or during 2019 fieldwork. We observed a few small surface lakes (<0.002 km^2) on the terminal lobe of Thores Glacier in 2019 (Fig. 10C), although they were only a few meters deep at most. No supraglacial lakes were present in 1959, according to the air photograph (Fig. 10A), but a 0.02 km^2 lake was present in 1984, the largest observed in our records (Fig. 10B).

Long-term changes in Thores Glacier

The northwest terminus of Thores Glacier advanced between 1959 and 2019, while the southeast terminus, which ends in Thores Lake, retreated (Figs. 2 and 10). The southeast terminus retreated by a maximum of 130 m over this period, with the air photographs showing that most of this occurred between 1984 and 2019. The northwest terminus advanced by a maximum of 170 m between 1959 and 2019, although due to the omission of this part of the terminus in the 1984 air photograph and lack of other high-resolution satellite imagery, we are unable to determine whether the rate of advance has varied since 1959 (Fig. 10).

Fig. 8. View of ice cliffs at the northwest terminus of Thores Glacier, taken from a helicopter on 15 July 2019. For scale, Thores Glacier valley is approximately 1.4 km wide in this photo. Ice cliffs are approximately 20 m high.

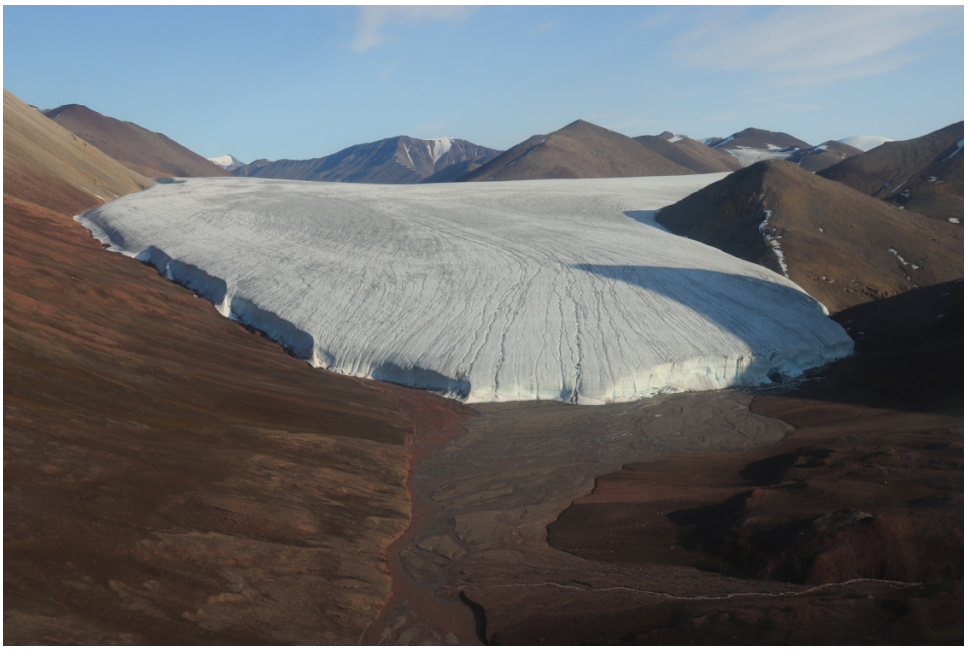

Fig. 9. Snow bridge (~50 m long) and emerging supraglacial stream observed on 15 July 2019. Location of photograph shown in Fig. 2.

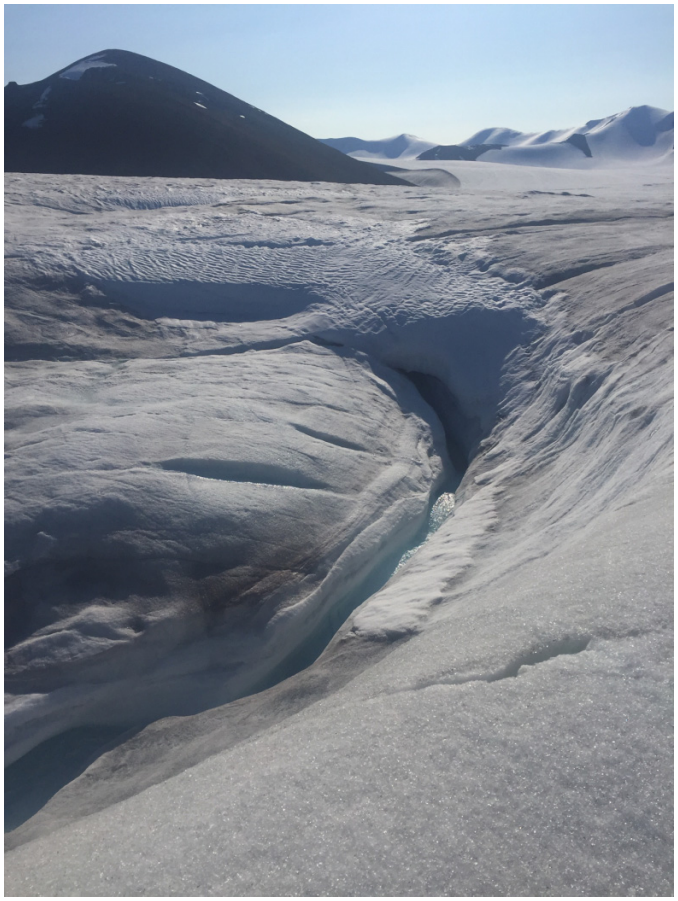

We found no evidence of change within the uncertainty of our methods along the northern margin of the terminal lobe (Fig. 2).

While the supraglacial streams are difficult to see in the 1959 air photograph, there was little evidence of significant changes in their extent or distribution up to the present day. Some streams have shifted in position slightly, while one on the southeast margin now leaves the glacier 1.5 km further down-glacier than it used to due to changes in the surface slope, rather than advection due to ice motion (Fig. 2).

We found evidence of only minor retreat in glacier extent since the Little Ice Age based on the distance between a distinct change in bedrock colour around the margins of the glacier (Fig. 11). As described by previous studies in the Canadian Arctic such as Ives (1962), Locke and Locke (1977), and Wolken (2006), this change in surficial colour is typically due to the lack of lichens, vegetation, and weathering in past ice-covered areas, and can be used to map the Little Ice Age maximum ice extent. This transition is most noticeable on either side of Thores Lake near the southeast glacier margin (Fig. 11C), and in most locations we found a maximum distance of 60 m, but more typically 20–30 m, between the modern glacier margin and the hypothesized Little Ice Age extent (Fig. 11). Most studies assign an end date of ~1850–1900 to the Little Ice Age in the Canadian Arctic (e.g., Barry and Hall-McKim 2019). While we observed the most evidence for change near to the northwest and southeast termini, we are unable to quantify how the termini themselves changed since the Little Ice Age, since the northwest portion has advanced over any previous evidence and the southeast portion is in Thores Lake.

Fig. 10. Air photographs of the lower ablation area of Thores Glacier. The blue line shows the extent of the glacier in 2019, with the line thickness representing the measurement uncertainty. (A) 26 July 1959 (photo A16694-112). (B) 29 July 1984 (photo A26575-007); note that there is poor alignment on the western margin of the glacier in this photograph due to lack of ground control points. (C) Orthomosaic from our 28 July 2019, air photograph survey. Supraglacial lakes are present in the central part of the lower terminus in parts (B, C).

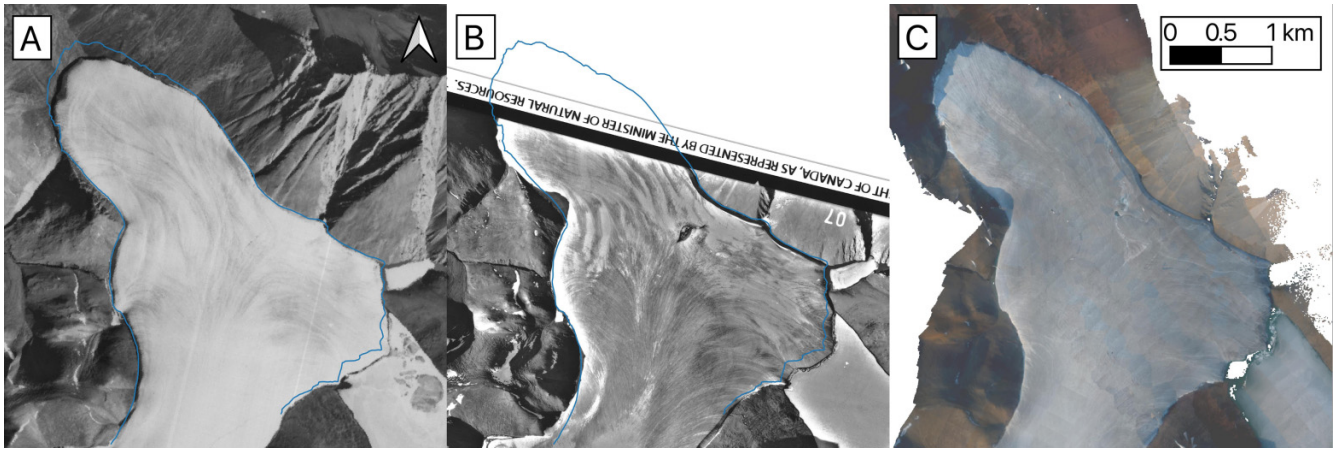

Glacier velocity and basal temperature

In terms of overall velocity, Thores Glacier is moving slowly (Fig. 5), with a median velocity over the entire glacier of 7.43 ± 1.8 m a^{-1} based on velocity maps from 2016 to 2021. The fastest velocities occur in the throat of the glacier, the narrowest area located 630–800 m a.s.l., with a median of 14.4 ± 1.8 m a^{-1} and peak of 26 ± 1.8 m a^{-1}. The lobe, the area below 630 m a.s.l. is slower with a median of 7.31 ± 1.8 m a^{-1}. The lower (800–950 m a.s.l.) and upper accumulation areas (above 950 m a.s.l.) have median velocities of 7.03 ± 1.8 m a^{-1} and 7.35 ± 1.8 m a^{-1}, respectively. The velocities of Thores Glacier are generally lower than those of other land-terminating glaciers of a similar size in the Canadian Arctic where previous measurements have been made, of ~20–40 m a^{-1} in the ablation area of John Evans Glacier (350 km south; Bingham et al. 2006) and White Glacier (460 km southwest; Iken 1972; Thomson and Copland 2017). The low velocity suggests that the glacier is frozen to its bed.

Frozen basal conditions were confirmed by the 1-D temperature modelling, which suggests a basal temperature of −9.1 °C to −13.8 °C for conditions at the equilibrium line and lower accumulation area, assuming a mean annual surface temperature of −18.5 °C, ice thickness of 360 m, and vertical velocity varying between 0.0 and −0.5 m a^{-1}. In the lower terminus region, the basal ice temperature was estimated to be −8.8 °C for an ice thickness of 200 m, vertical velocity of +0.5 m a^{-1}, and mean annual surface temperature of −18.5 °C. For a model run with a mean annual surface temperature of −16.7 °C and the other boundary conditions kept constant, the predicted basal temperatures increased by a few degrees (−7.2 °C to −12.0 °C at the equilibrium line and lower accumulation area, −7.0 °C over the lower terminus), but were still well below freezing. The neglect of horizontal diffusion in the model likely makes little difference to the results, while the neglect of horizontal advection means that modelled basal temperatures are likely a maximum value, as Wohlleben et al. (2009) demonstrated that the inclusion of horizontal advection would cool the glacier interior and bed due to the downdraw of cold near-surface firn from the accumulation zone.

As an additional check on the presence of frozen basal conditions, surface velocities were computed using a vertical integration of Glen's flow law under the shallow ice approximation (equation 2 in Wohlleben et al. 2009), using a flow law parameter consistent with the ice temperatures modelled above and measured ice depths at Thores Glacier. Spot checks with this equation along the glacier centreline reveal that the measured surface velocities are consistent with zero horizontal motion at the bed (i.e., no basal sliding).

Relationship between Thores Glacier and Thores Lake

Thores Glacier currently acts as a dam, and is the only reason that proglacial Thores Lake exists. The current surface of Thores Lake is 80 m above the bed of the adjacent glacier ice at the southeast terminus of Thores Glacier, and 150 m above the northwest terminus of the glacier (Fig. 6C). Thus, in its current position, Thores Glacier is acting as a dam and without the glacier there would be no lake. Furthermore, if the glacier were to retreat and (or) thin enough, the lake would drain to the north, resulting in all meltwater from the glacier flowing in that direction, rather than the current split between north and southeast. It is possible that there could be some places under the current terminal lobe of the glacier where a new lake could form, but our GPR data lack the spatial coverage to make such a determination.

Discussion

Long-term stability of Thores Glacier

Overall, there is evidence for minimal change around the perimeter of Thores Glacier since the Little Ice Age, with changes in bedrock colour suggesting a maximum total

Fig. 11. Photos of the boundary between weathered and unweathered bedrock (indicated by white arrows) around the margins of Thores Glacier, hypothesized to mark the Little Ice Age extent. (A) Viewshed or extent of (B–D). (B) Ground view on the north side on 23 July 2019. (C) Aerial view from a helicopter on 28 July 2019. (D) Ground view on the south side across Thores Lake on 23 July 2019.

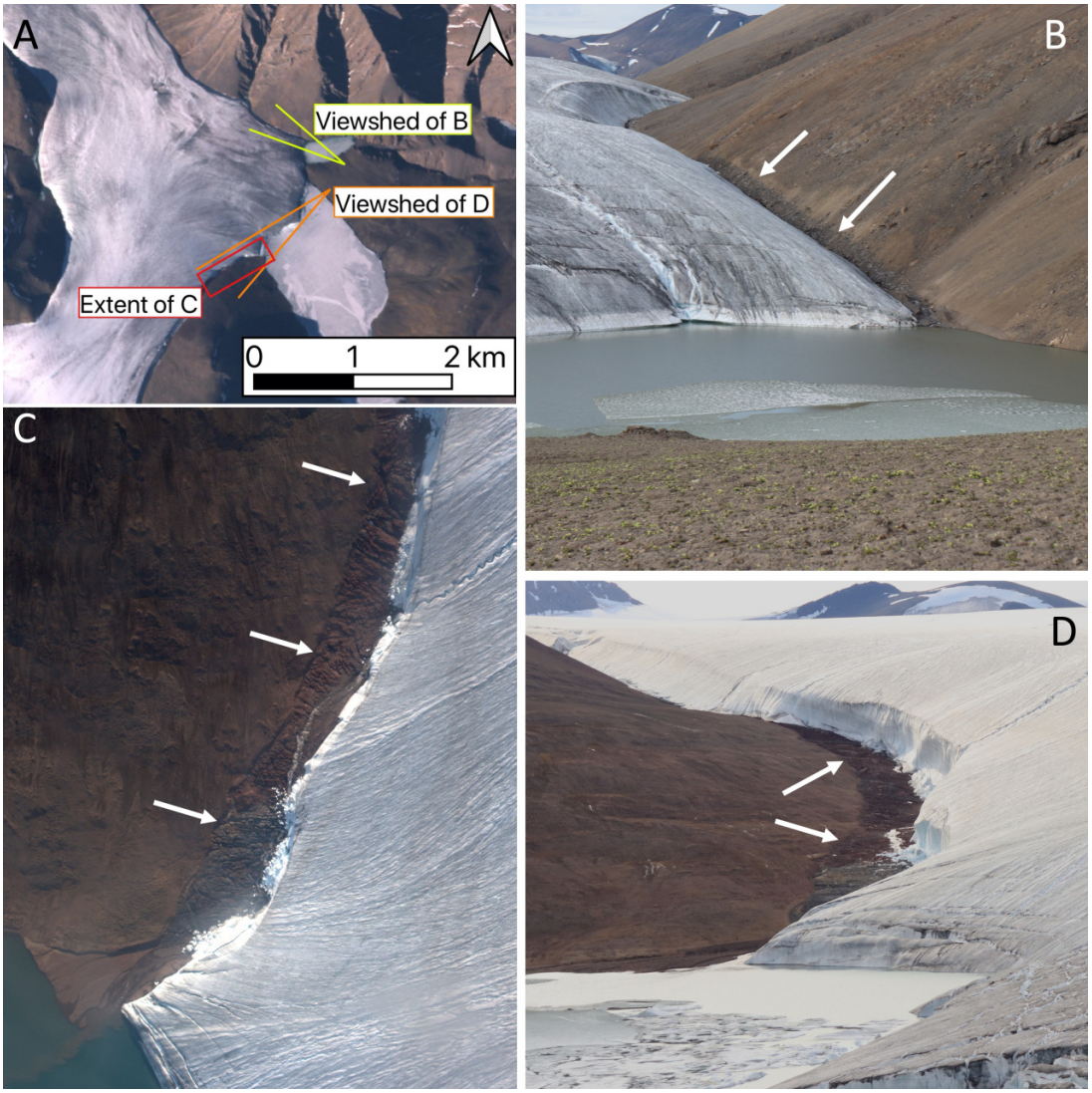

retreat of 20–30 m for most locations where such evidence is available. This is consistent with the advance of the northwest terminus by up to 170 m since 1959, and the present-day accumulation area ratio of 0.77 (Fig. 4). There are few other glaciers in this region where the accumulation area ratio has been determined, but Thomson et al. (2017) report that the mean accumulation area ratio at White Glacier between 1960 and 2015 was 0.55 during a period of increasingly negative mass balance. Based on a global analysis, Dyurgerov et al. (2009) report that equilibrium accumulation area ratio values (i.e., those indicative of a glacier with a neutral mass balance) vary between about 0.40 and 0.80, with an overall mean of 0.579 ± 0.09. This suggests that the 0.77 value for Thores Glacier is representative of a glacier near steady-state, or perhaps with a positive mass balance.

Based on these patterns, the retreat of the southeast terminus by up to 130 m, primarily between 1984 and 2019, may be due to changes in Thores Lake during this period. Long-term limnological data are unavailable for this lake, but studies at Ward Hunt Lake, 45 km to the north, have shown a rapid warming trend, with 4.2 m thick summer lake ice thinning in the early 21st century, resulting in unprecedented open water conditions in 2011 (Paquette et al. 2015). Ward Hunt Lake also experienced extreme warming, open water and anomalous limnological conditions in 2016 (Bégin et al. 2021), and this late summer event could have affected Thores Lake.

No in situ measurements of surface mass balance exist for land-terminating glaciers on far northern Ellesmere Island, although some measurements do exist for the ice shelves and associated ice rises along the northern coastline. The nearest of these is Ward Hunt Ice Rise (WHIR) and Ward Hunt Ice Shelf (WHIS), located ~50 km to the north of Thores Glacier. The WHIR lost a total of 1.68 m water equivalent

(w.e.) between 1959 and 2005, which equates to a mean surface mass balance of −0.04 m w.e. a^{-1}, while the WHIS had a mean surface mass balance of −0.07 m w.e. a^{-1} over the same period (Braun et al. 2004*b*; Braun 2017). Rates appear to have increased recently, with losses in a single year reaching up to 0.33 m w.e. on WHIR and 0.54 m w.e. on WHIS in 2003, although that summer was exceptionally warm. Even though these ice masses are in a more maritime setting and at lower elevation than Thores Glacier, they suggest that surface mass balance in this region at low elevations has been only slightly negative over most of the period between the 1950s and present day.

Regional atmospheric climate model results at 1 km resolution by Noël et al. (2018) suggest that Thores Glacier has experienced an increasingly positive mass balance during recent times. Their results suggest a glacier-wide positive mass balance of 0.12 m w.e. a^{-1} for 1958–1995 and 0.13 m w.e. a^{-1} for 1996–2015, although there are large losses at the northwest terminus of ∼0.60 m w.e. a^{-1}. This modelled net mass gain is consistent with our observations of advance of the NW terminus during this period. However, recent geodetic mass balance observations for 2000–2019 of Thores Glacier suggest a glacier average surface elevation change of −0.16 m w.e. a^{-1} (Hugonnet et al. 2021), although there are potentially high errors in these measurements due to the lack of local measurements and therefore interpolation of elevation change values from elsewhere. Noël et al. (2018) report that the mean regional surface mass balance for the entire Queen Elizabeth Islands was −0.08 m w.e. a^{-1} for 1958–1995 and −0.24 m w.e. a^{-1} for 1996–2015. Similarly, mean glacier-wide surface mass balance at White Glacier over the period 1960–2014 ranged between −0.18 and −0.21 m w.e. a^{-1} for geodetic and glaciological (i.e., in situ) measurements, respectively (Thomson et al. 2017). Thus, Thores Glacier is unusual in that it is one of the few known glaciers in the Queen Elizabeth Islands to have experienced a positive mass balance over the past 50+ years, although the results of Hugonnet et al. (2021) suggest that it may have already transitioned to a negative mass balance in recent times. The hypsometry of Thores Glacier, where most of the glacier area is above the equilibrium line (Fig. 4), likely contributes to this relative stability.

Hydrological and thermal structure of Thores Glacier

Thores Glacier currently has a poorly developed supraglacial drainage network, with a limited number of streams that direct meltwater to drain off the glacier margins in the ablation zone. There are currently no moulins on Thores Glacier, and few crevasses, and therefore no evidence of meltwater reaching the glacier interior or bed. This contrasts with observations of well-developed supraglacial drainage networks with deeply incised channels on glaciers in more southerly locations in the Canadian Arctic, and associated water flow to their glacier interior and bed through moulins and crevasses, such as at John Evans Glacier (Skidmore and Sharp 1999; Bingham et al. 2006), and White Glacier (Iken 1972; Thomson and Copland 2017).

Future evolution and changes at Thores Glacier

The most effective way to warm the bed of Thores Glacier, and therefore to speed it up, would be to bring water to the bed (Hutter 1993; Wohlleben et al. 2009). Seasonal increases in basal water pressure at other glaciers in more southerly locations in the Queen Elizabeth Islands has led to marked increases in surface velocity, such as at White Glacier (Thompson and Copland 2017) and John Evans Glacier (Bingham et al. 2006). One supraglacial stream at Thores Glacier is currently englacial for a short distance (∼50 m) due to a snow bridge and steep stream banks (Fig. 9), which may provide a mechanism to create a moulin, but melt would need to increase significantly for this to occur as the ice is over 200 m thick along the centerline, some 500 m to the west. For the bed to reach the melting point without the formation of a new moulin would require a significant increase in mean annual air temperature of at least 5 °C to 7 °C above present, and decades to centuries for that temperature increase to be advected to the glacier bed through vertical ice motion. Given the slightly positive mass balance in recent decades found in modelling studies (Noël et al. 2018), and little change in the glacier margins since the Little Ice Age, Thores Glacier appears to be relatively stable.

Future changes to the subglacial hydrologic system could also impact proglacial Thores Lake and local drainage patterns. Given that Thores Glacier is currently acting as a dam for Thores Lake, future climate warming and ice attrition could dramatically alter water movement in the region. Loss or breaching of the ice dam would result in the complete disappearance of the lake ecosystem, and the creation of an altered flowing water ecosystem to the north. Proglacial lakes are well known in the geological record for their sensitivity to climate fluctuations, most dramatically in the case of proglacial Lake Agassiz and its associated megafloods (Fisher 2020). Lake level drop and catastrophic drainage have been reported elsewhere in the northern Ellesmere Island region, for an ice-dammed lake that feeds into Lake Tuborg at latitude 80.95°N (Lewis et al. 2009). With ongoing rapid climate change in the region, including extreme warming events, the Thores proglacial lake system is more likely to be pushed from its current stability to the brink of ice dam collapse, lake drainage, and associated reconfiguration of the entire hydrological system.

Conclusions

The measurements at Thores Glacier indicate a glacier system which has been relatively stable over the past century, and which has changed little recently despite large losses reported on glaciers and ice caps to the south (Braun et al. 2004*a*; Serreze et al. 2017; White and Copland 2018), and ice shelves and a coastal glacier to the north (Copland and Mueller 2017; White and Copland 2018; Tsuji et al. 2022). This stability is consistent with the findings of White and Copland (2018), who reported no detectable change for Thores Glacier and most land-terminating glaciers in the Disraeli Fiord region to the south of the WHIS between ∼1999 and 2015. Evidence from slow surface velocities, a poorly developed

supraglacial stream network, a lack of moulins, lack of internal reflections in GPR measurements (Fig. 7), and basal temperature modelling suggests that Thores Glacier, and likely others nearby, are true polar glaciers with ice frozen to the bed across their entire extent. This contrasts with glaciers of a similar size in slightly more southerly locations in the Canadian Arctic, such as John Evans Glacier (79.66°N; Copland and Sharp 2001) and White Glacier (79.50°N; Blatter 1987), which contain moulins and have been shown to have polythermal basal conditions across the lower part of their ablation areas.

The lowest ELAs in the northern hemisphere occur along the northern coast of Ellesmere Island (Miller et al. 1975), making the glaciers in this region one of the last vestiges of polar glaciers in the world outside Antarctica. This is supported by the glacial geological observations of Evans (1989), who argued that the lack of englacial debris in folia in glacier termini in Philips Inlet, 200 km west of Thores Glacier, is indicative of ice that has not experienced basal freeze-on, in contrast to locations such as southern Baffin Island (Dowdeswell 1986) or Svalbard (Boulton 1970). Lemmen (1989) used evidence from ice-marginal landforms and radiocarbon dating to argue for a relatively limited ice cover over the Marvin Peninsula during the last glaciation due to the arid climate there, with glaciers only advancing up to 20 km beyond their present margins, suggesting that there has been general long-term stability of land-terminating ice masses in this region.

Despite the recent stability of Thores Glacier, it is likely that changes at the glacier will accelerate over the coming decades as the climate warms and the Arctic continues to change. A rise in the ELA by 200 m above present, similar to that recorded at White Glacier between 1960 and 2014 (Thomson et al. 2017), would cause the accumulation area ratio to reduce from 0.77 to 0.46 (Fig. 4), which would likely push the glacier into a state of strongly negative surface mass balance. This negative mass balance and associated increase in surface melt, together with atmospheric warming, has the potential to lead to warming of the glacier bed to the melting point, which is of particular concern across the lower terminus where it currently dams Thores Lake. With the glacier bed 80–150 m below the current surface of Thores Lake, there is the potential for this lake to drain beneath the glacier if it reaches the melting point, or around the northern margin if the ice retreats enough. If this were to occur, it would completely change the regional drainage system and send all water through the valley to the northwest of Thores Glacier. This would lead to the disappearance of Thores Lake and its associated ecosystems.

Acknowledgements

We thank the Polar Continental Shelf Program, Natural Sciences and Engineering Research Council of Canada, ArcticNet Network of Centres of Excellence Canada, Canada Research Excellence Fund Sentinel North, Canada Foundation for Innovation, Ontario Research Fund, Vanier Canada Graduate Scholarship, Centre d'études nordiques and University of Ottawa for funding to complete this work. We thank Derek Mueller for the loan of his GPR unit, and Denis Sarrazin, Elise Imbeau, Steven Page, and Steven Crerar for their assistance during fieldwork. We also thank Parks Canada and Centre d'études nordiques for the use of facilities on Ward Hunt Island, and the Nunavut Research Institute, Parks Canada, and the communities of Aujuittuq (Grise Fiord) and Qausuittuq (Resolute Bay) for permission to undertake the fieldwork in this area. We thank the editors of Arctic Science, Doug Brinkerhoff and an anonymous reviewer for comments which helped to improve this paper.

Article information

History dates

Received: 20 February 2022
Accepted: 25 August 2022
Version of record online: 11 November 2022

Notes

This paper is part of a Collection entitled "Terrestrial Geosystems, Ecosystems, and Human Systems in the Fast-Changing Arctic".

Copyright

Data availability

The photogrammetry data sets we generated and our glacier thickness estimates are available from the Polar Data Catalogue under CCIN reference number 13275 (https://www.polardata.ca/pdcsearch/?doi_id=13275). Air photos used in this study are available from the National Air Photo Library, Ottawa, Canada. All satellite imagery used in this study is publicly available from data sources listed in the methods.

Author information

Author ORCIDs

Will Kochtitzky https://orcid.org/0000-0001-9487-1509
Catherine Girard https://orcid.org/0000-0002-3899-0180
Warwick F. Vincent https://orcid.org/0000-0001-9055-1938
Alexander I. Culley https://orcid.org/0000-0001-6639-9112

Author notes

Warwick F. Vincent served as an Associate Editor at the time of manuscript review and acceptance; peer review and editorial decisions regarding this manuscript were handled by Julia Boike and Greg Henry.

Author contribution

W.K.: Conceptualization, data curation, formal analysis, investigation, methodology, visualization, writing – original draft, writing – review & editing. L.C.: Conceptualization, methodology, resources, supervision, writing – origi-

nal draft, writing – review & editing. T.W.: Formal analysis, investigation, methodology. P.I.: Investigation. C.G.: Conceptualization, investigation, writing – review & editing. W.F.V.: Conceptualization, project administration, resources, supervision, writing – review & editing. A.I.C.: Conceptualization, data curation, funding acquisition, investigation, methodology, project administration, resources, supervision, writing – review & editing.

Competing interests

The authors declare there are no competing interests.

References

Barry, R.G., and Hall-McKim, E.A. 2019. Polar environments and global change. Cambridge University Press, Cambridge. doi:10.1017/9781108399708.

Bégin, P. N., Tanabe, Y., Kumagai, M., Culley, A. I., Paquette, M., Sarrazin, D., et al. 2021. Extreme warming and regime shift toward amplified variability in a far northern lake. Limnology and Oceanography, **66**: S17–S29. doi:10.1002/lno.11546.

Beltrami, H., and Taylor, A.E. 1995. Records of climatic change in the Canadian Arctic: towards calibrating oxygen isotope data with geothermal data. Global and Planetary Change, **11**(3): 57–70. doi:10.1016/0921-8181(95)00006-2.

Bingham, R.G., Nienow, P.W., Sharp, M.J., and Boon, S. 2005. Subglacial drainage processes at a High Arctic polythermal valley glacier. Journal of Glaciology, **51**(172): 15–24. doi:10.3189/172756505781829520.

Bingham, R., Nienow, P., Sharp, M., and Copland, L. 2006. Hydrology and dynamics of a polythermal (mostly cold) High Arctic glacier. Earth Surface Processes and Landforms, **31**: 1463–1479. doi:10.1002/esp.1374.

Blatter, H. 1987. On the thermal regime of an Arctic valley glacier: a study of White Glacier, Axel Heiberg Island, N.W.T., Canada. Journal of Glaciology, **33**(114): 200–211. doi:10.3189/S0022143000008704.

Bogorodsky, V. V., Bentley, C.R., and Gudmandsen, P.E. 1985. Radioglaciology. D. Reidel Publishing Company, Dordrecht, Netherlands. doi:10.1007/978-94-009-5275-1.

Boulton, G.S. 1970. On the origin and transport of englacial debris in Svalbard Glaciers. Journal of Glaciology, **9**(56): 213–229. doi:10.3189/S0022143000023534.

Braun, C. 2017. The surface mass balance of the Ward Hunt Ice Shelf and Ward Hunt Ice Rise, Ellesmere Island, Nunavut, Canada. *In* Arctic ice shelves and ice islands, Chapter 6. *Edited by* L. Copland and D. Mueller. Springer Nature, Dordrecht. pp.149–183. doi:10.1007/978-94-024-1101-0_6.

Braun, C., Hardy, D.R., and Bradley, R.S. 2004a. Mass balance and area changes of four High Arctic plateau ice caps. Geografiska Annaler, **86A**(1): 43–52. doi:10.1111/j.0435-3676.2004.00212.x.

Braun, C., Hardy, D.R., Bradley, R.S., and Sahanatien, V. 2004b. Surface mass balance of the Ward Hunt Ice Rise and Ward Hunt Ice Shelf, Ellesmere Island, Nunavut, Canada. Journal of Geophysical Research: Atmospheres, **109**(D22): D22110. doi:10.1029/2004JD004560.

Casey, J.A., and Kelly, R.E. 2010. Estimating the equilibrium line of Devon Ice Cap, Nunavut, from RADARSAT-1 ScanSAR wide imagery. Canadian Journal of Remote Sensing, **36**: S41–S55. doi:10.5589/m10-013.

Centre d'études Nordiques (Centre for Northern Studies (CEN)). 2020. Climate station data from northern Ellesmere Island in Nunavut, Canada, v. 1.7 (2002–2019). Nordicana D1. doi:10.5885/44985SL-8F203FD3ACCD4138.

Ciracì, E., Velicogna, I., and Swenson, S. 2020. Continuity of the mass loss of the world's glaciers and ice caps from the GRACE and GRACE follow-on missions. Geophysical Research Letters, **47**(9): e2019GL086926. doi:10.1029/2019GL086926.

Copland, L., and Sharp, M. 2001. Mapping thermal and hydrological conditions beneath a polythermal glacier with radio-echo sounding. Journal of Glaciology, **47**(157): 232–242. doi:10.3189/172756501781832377.

Copland, L., and Mueller, D. (eds.). 2017. Arctic ice shelves and ice islands. Springer Nature, Dordrecht. 425 pp. doi:10.1007/978-94-024-1101-0.

Copland, L., and Mueller, D. 2021. Climate station data from Purple Valley at the head of Milne Fiord, northern Ellesmere Island, Nunavut, Canada, v. 1 (2009-2019). Nordicana D93. doi:10.5885/45735XD-011EA11523034D87.

Culley, A., Thaler, M., Kochtitzky, W., Iqaluk, P., Rapp., J., Rautio, M., et al. 2022. The Thores Lake proglacial system: remnant stability in the rapidly changing Canadian High Arctic. Arctic Science. In press. doi:10.1139/as-2022-0023.

Dehecq, A., Gourmelen, N., and Trouve, E. 2015. Deriving large-scale glacier velocities from a complete satellite archive: application to the Pamir-Karakoram-Himalaya. Remote Sensing of Environment, **162**: 55–66. doi:10.1016/j.rse.2015.01.031.

Dowdeswell, J.A. 1986. The distribution and character of sediments in a tidewater glacier, southern Baffin Island, N.W.T., Canada. Arctic and Alpine Research, **18**(1): 45–56. doi:10.1080/00040851.1986.12004062.

Dyurgerov, M., Meier, M.F., and Bahr, D.B. 2009. A new index of glacier area change: a tool for glacier monitoring. Journal of Glaciology, **55**(192): 710–716. doi:10.3189/002214309789471030.

Evans, D.J.A. 1989. Apron entrainment at the margins of sub-polar glaciers, north-west Ellesmere Island, Canadian High Arctic. Journal of Glaciology, **35**(121): 317–324. doi:10.3189/S0022143000009230.

Fisher, T.G., 2020. Megaflooding associated with glacial lake agassiz. Earth-Science Reviews, **201**: 102974. doi:10.1016/j.earscirev.2019.102974.

Hugonnet, R., McNabb, R., Berthier, E., Menounos, B., Nuth, C., Girod, L., et al. 2021. Accelerated global glacier mass loss in the early twenty-first century. Nature, **592**: 726–731. doi:10.1038/s41586-021-03436-z. PMID: 33911269.

Hutter, K. 1993. Thermo-mechanically coupled ice-sheet response – cold, polythermal, temperate. Journal of Glaciology, **39**(131): 65–86. doi:10.1017/S0022143000015720.

Iken, A. 1972. Measurements of water pressure in Moulins as part of a movement study of the White Glacier, Axel Heiberg Island, Northwest Territories, Canada. Journal of Glaciology, **11**(61): 53–58. doi:10.3189/S0022143000022486.

Iken, A. 1974. Velocity fluctuations of an arctic valley glacier. A study of the White Glacier, Axel Heiberg Island, Canadian Arctic Archipelago. Glaciology, **5**: 123. Axel Heiberg Island Research Reports.

Ives, J. 1962. Indications of recent extensive glacierization in north-central Baffin Island, N.W.T. Journal of Glaciology, **4**(32): 197–205. doi:10.3189/S0022143000027398.

Krumwiede, B. S., Kamp, U., Leonard, G. J., Kargel, J. S., Dashtseren, A., and Walther, M. 2014. Recent glacier changes in the Mongolian Altai Mountains: case studies from Munkh Khairkhan and Tavan Bogd. *In* Global land ice measurements from space. *Edited by* J. Kargel, G. Leonard, M. Bishop and A. Kääb. Springer, Berlin. pp. 481–508. doi:10.1007/978-3-540-79818-7_22.

Lei, Y, Gardner, A., and Agram, P. 2021. Autonomous repeat image feature tracking (autoRIFT) and its application for tracking ice displacement. Remote Sensing, **13**(4): 749. doi:10.3390/rs13040749.

Lemmen, D.S. 1989. The last glaciation of Marvin Peninsula, northern Ellesmere Island, High Arctic, Canada. Canadian Journal of Earth Sciences, **26**(12): 2578–2590. doi:10.1139/e89-220.

Lewis, T., Francus, P., and Bradley, R.S. 2009. Recent occurrence of large jökulhlaups at Lake Tuborg, Ellesmere Island, Nunavut. Journal of Paleolimnology, **41**: 491. doi:10.1007/s10933-008-9240-4.

Locke, C.W., and Locke, W.W. 1977. Little ice age snow-cover extent and paleoglaciation thresholds: north-central Baffin Island, N.W.T., Canada. Arctic and Alpine Research, **9**: 291–300. doi:10.2307/1550544.

Miller, G.H., Bradley, R.S., and Andrews, J.T. 1975. The glaciation level and lowest equilibrium line altitude in the high Canadian Arctic: maps and climatic interpretation. Arctic and Alpine Research, **7**(2): 155–168. doi:10.2307/1550318.

Mortimer, C.A., Copland, L., and Mueller, D.R. 2012. Volume and area changes of the Milne Ice Shelf, Ellesmere Island, Nunavut, Canada, since 1950. Journal of Geophysical Research: Earth Surface, **117**(F4): F04011. doi:10.1029/2011JF002074.

Mueller, D.R., Vincent, W.F., and Jeffries, M.O. 2003. Break-up of the largest Arctic ice shelf and associated loss of an epishelf lake. Geophysical Research Letters, **30**(20): 2031. doi:10.1029/2003GL017931.

Newton, R., Pfirman, S., Tremblay, L.B., and DeRepentigny, P. 2021. Defining the "ice shed" of the Arctic Ocean's last ice area and its future evolution. Earth's Future, **9**: e2021EF001988. doi:10.1029/2021EF001988.

Noël, B.P.Y. 2017. Average surface mass balance (SMB) components at 1 km for the Canadian Arctic Archipelago (1958-1995 and 1996-2015), links to RACMO2.3 model results in NetCDF format. PANGAEA, doi:10.1594/PANGAEA.881315.

Noël, B.P.Y., van de Berg, W.J., Lhermitte, S., Wouters, B., Schaffer, N., and van den Broeke, M.R. 2018. Six decades of glacial mass loss in the Canadian Arctic Archipelago. Journal of Geophysical Research: Earth Surface, **123**(6): 1430–1449. doi:10.1029/2017JF004304.

Northern Ellesmere Island in the Global Environment (NEIGE). 2020. Dynamics of ice cover over a far northern lake: direct observations of Ward Hunt Lake, Canadian High Arctic, by automated camera, v. 1.1 (2016-2019). Nordicana D74. doi:10.5885/45648CE-1A9AB63DFF91440B.

Paquette, M., Fortier, D., Mueller, D.R., Sarrazin, D., and Vincent, W.F. 2015. Rapid disappearance of perennial ice on Canada's most northern lake. Geophysical Research Letters, **42**: 1433–1440. doi:10.1002/2014GL062960.

Porter, C., Morin, P., Howat, I., Noh, M., Bates, B., Peterman, K., et al. 2018. ArcticDEM. Harvard Dataverse, V1. doi:10.7910/DVN/OHHUKH [accessed 4 November 2021].

Randolph Glacier Inventory (RGI) Consortium. 2017. Randolph glacier inventory – a dataset of global glacier outlines: version 6.0. Technical Report, Global land ice measurements from space, Digital Media, Colorado, USA. doi:10.7265/N5-RGI-60.

Serreze, M.C., Raup, B., Braun, C., Hardy, D.R., and Bradley, R.S. 2017. Rapid wastage of the hazen plateau ice caps, northeastern Ellesmere Island, Nunavut, Canada. The Cryosphere, **11**: 169–177. doi:10.5194/tc-11-169-2017.

Sharp, M., Burgess, D.O., Cogley, J.G., Ecclestone, M., Labine, C., and Wolken, G.J. 2011. Extreme melt on Canada's Arctic ice caps in the 21st century. Geophysical Research Letters, **38**: L11501. doi:10.1029/2011GL047381.

Skidmore, M.L., and Sharp, M.J. 1999. Drainage system behaviour of a high-arctic polythermal glacier. Annals of Glaciology, **28**: 209–215. doi:10.3189/172756499781821922.

Tepes, P., Gourmelen, N., Nienow, P., Tsamados, M., Shepherd, A., and Weissgerber, F. 2021. Changes in elevation and mass of Arctic Glaciers and ice caps, 2010-2017. Remote Sensing of the Environment, **261**: 112481. doi:10.1016/j.rse.2021.112481.

Thomson, L., and Copland, L. 2016. White glacier 2014, axel heiberg island, nunavut: mapped using structure from motion methods. Journal of Maps, **12**(5): 1063–1071. doi:10.1080/17445647.2015.1124057.

Thomson, L., and Copland, L. 2017. Multi-decadal reduction in glacier velocities and mechanisms driving deceleration at polythermal White Glacier, Arctic Canada. Journal of Glaciology, **63**(239): 450–463. doi:10.1017/jog.2017.3.

Thomson, L., Zemp, M., Copland, L., Cogley, G., and Ecclestone, M. 2017. Comparison of geodetic and glaciological mass budgets for White Glacier, Axel Heiberg Island, Canada. Journal of Glaciology, **63**(237): 55–66. doi:10.1017/jog.2016.112.

Tsuji, M., Vincent, W.F., Tanabe, Y., and Uchida, M. 2022. Glacier retreat results in loss of fungal diversity. Sustainability, **14**: 1617. doi:10.3390/su14031617.

Vincent, W.F., and Mueller, D. 2020. Witnessing ice habitat collapse in the Arctic. Science **370**: 1031–1032. doi:10.1126/science.abe4491. PMID: 33243873.

Vincent, W.F., Canário, J., and Boike, J. 2019. Understanding the terrestrial effects of Arctic Sea ice decline. Eos, **100**. doi:10.1029/2019EO128471.

Vincent, W.F., Fortier, D., Lévesque, E., Boulanger-Lapointe, N., Tremblay, B. Sarrazin, D., et al. 2011. Extreme ecosystems and geosystems in the Canadian High Arctic: Ward Hunt Island and vicinity. Écoscience, **18**: 236–261. doi:10.2980/18-3-3448.

White, A., and Copland, L. 2018. Area change of glaciers across northern Ellesmere Island, Nunavut, between ~1999 and ~2015. Journal of Glaciology, **64**(246): 609–623. doi:10.1017/jog.2018.49.

Wohlleben, T., Sharp, M., and Bush, A. 2009. Factors influencing the basal temperatures of a High Arctic polythermal glacier. Annals of Glaciology, **50**(52): 9–16. doi:10.3189/172756409789624210.

Wolken, G.J. 2006. High-resolution multispectral techniques for mapping former little ice age terrestrial ice cover in the Canadian High Arctic. Remote Sensing of Environment, **101**(1): 104–114. doi:10.1016/j.rse.2005.12.009.